In Proceedings of Oceans '95 MTS/IEEE, San Diego, October, 1995.

Experiments in the Coordination of Underwater Manipulator and Vehicle Control

Timothy W. McLain* Stephen M. Rock†
Stanford University Aerospace Robotics Laboratory
Durand Building 250
Stanford, California 94305

Michael J. Lee‡
Monterey Bay Aquarium Research Institute
160 Central Avenue
Pacific Grove, California 93950

Abstract

Experiments using the OTTER vehicle conducted at the Monterey Bay Aquarium Research Institute (MBARI) have shown that dynamical interactions between a robotic arm and an underwater vehicle can be very significant due to the hydrodynamic forces acting on the arm as it moves through the water. Using a new, highly-accurate model of these hydrodynamic interaction forces, which was developed as part of this research, a coordinated arm/vehicle control strategy was implemented. Under this model-based approach, interaction forces acting on the vehicle due to arm motion were predicted and fed forward into the vehicle control system. Using this method, vehicle station-keeping capability was greatly enhanced. Tracking errors and settling times for the manipulator end point were reduced significantly.

1 Introduction

For users of remotely operated vehicles (ROVs), manipulators have become a valuable tool for performing a wide variety of tasks from scientific sampling to maintenance and construction of underwater structures. Unlike ROVs, which tend to be quite stable statically, many smaller underwater vehicles have reduced static stability due to the small separation distance between their centers of gravity and buoyancy. The addition of manipulators to the vehicle makes control of the system more difficult because of the large hydrodynamic forces acting on the arm as it moves through the water. Hydrodynamic forces on the arm couple into the vehicle system, increasing the difficulty of regulating the position and attitude of the vehicle.

With the advent and implementation of higher levels of autonomy in the control of underwater robotic systems, it is becoming possible to move faster and hence the relevance of hydrodynamic coupling is increased further. Human/machine interfaces incorporating increased autonomy, such as Task-Level Control [1], are capable of providing commands which exploit the full capabilities of manipulators for quick, precise motions. To enable high-performance control of a manipulator end point from a free-swimming vehicle base, low-level control systems that deal effectively with the complex hydrodynamics of fast motion must be developed. The development and implementation of such a controller is the focus of this paper.

Figure 1: OTTER Vehicle With Single-Link Arm

*Doctoral Candidate, tmclain@sun-valley.stanford.edu
†Associate Professor, rock@sun-valley.stanford.edu
‡Senior Research Engineer, lemi@mbari.org

For the coordinated arm/vehicle control experiments discussed in this paper, a single-link arm was mounted on the OTTER vehicle, which is shown in Figure 1 and discussed in Section 2. Under the coordinated-control approach, the vehicle feedback controller was augmented with information about the hydrodynamic interaction forces between the arm and the vehicle. This information was produced using a very accurate model (developed during this work) of the hydrodynamic forces acting on the single-link arm.

Although the single-link arm is quite simple mechanically, hydrodynamically it is very complex due to the unsteady, three-dimensional flows developed as the arm moves. Although it does not possess the functionality of a full manipulator, the single link allows testing and validation of the coordinated-control concept. It was necessary to develop a model because many of the unique hydrodynamic attributes of robotic motion (*e.g.* short unsteady swinging motions, end effects, etc.) had not been addressed by previously existing models. As hydrodynamic models for manipulators increase in sophistication to handle *accurately* multiple links and degrees of freedom, the control approach presented here can be extended easily to accommodate these systems.

Controlling underwater vehicles and robots to enable them to perform useful functions in the deep ocean represents a difficult problem that has challenged researchers for many years. Several researchers have investigated the application of sliding-mode control [2, 3] to enable robust control of nonlinear vehicle systems in the presence of uncertainties. Other research focussed on using adaptive or neural-network control methods to deal with uncertainty in the plant model [4, 5].

The work of Mahesh, Yuh, and Lakshmi [6] is of direct relevance to the coordinated arm/vehicle control approach taken in this research. In their work, an adaptive controller for coordinating vehicle and arm motion was proposed. The success of their approach is dependent on the controller's ability to adapt accurately to rapidly changing hydrodynamic coefficients. The approach has been demonstrated using only a computer simulation of the planar motion of a vehicle.

Unlike the references presented here, the focus of this paper is not on increasing robustness or adapting to existing uncertainty, but rather on improving system performance by reducing the uncertainty of the system dynamics. The approach taken here involves augmenting the existing vehicle feedback control with model information based on a fundamental physical understanding of the manipulator hydrodynamics, in a way that benefits the control of the entire system.

2 Experimental Setup

The work presented here was performed as part of joint research program between the Stanford University Aerospace Robotics Laboratory (ARL) and the Monterey Bay Aquarium Research Institute (MBARI). To enable experimental research in the ARL/MBARI program, a small underwater vehicle has been developed. OTTER (an Ocean Technologies Testbed for Engineering Research) is described very briefly below, while further detail can be found in [7].

For the arm/vehicle coordinated control experiments presented in this paper a single-link arm was mounted on the OTTER vehicle. The OTTER vehicle is about 2.1 m long, 0.95 m wide, and 0.45 m tall and weighs about 145 kg in air. A cylindrical aluminum pressure housing, which contains the onboard computers and sensors, is the main structural element of the vehicle. Eight ducted, velocity-controlled thrusters provide propulsion to the vehicle. A schematic diagram of the various components of the OTTER vehicle is shown in Figure 2.

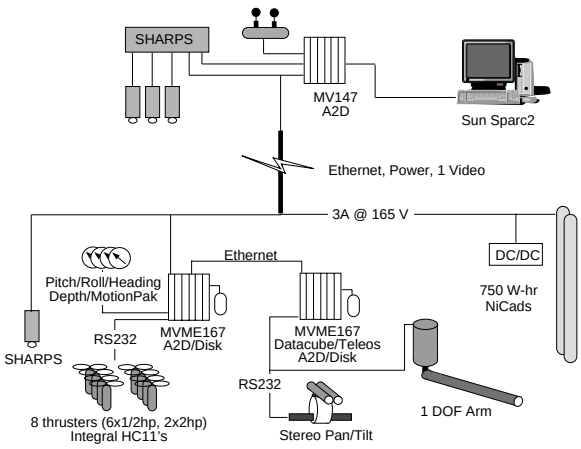

Figure 2: OTTER Hardware Architecture

The arm used for the control experiments was 0.071 m in diameter and 1.0 m long. This length was chosen because it has roughly the same effective length as the prototype manipulator that has been designed for OTTER when it is in a nominal operating configuration. The arm was mounted from the fore-port corner of the vehicle frame and tilted down at an angle of 60 degrees from the horizontal (see Figure 1). This configuration was chosen because it places the arm in the region most likely to be the workspace of a future manipulator.

With the arm mounted in this way, all of the vehicle degrees of freedom were affected by the forces generated as the arm moved.

In order to control the position and attitude of the vehicle, a variety of sensors were used. The horizontal (x, y) position of the vehicle was measured using SHARPS, an acoustic long-baseline positioning system. The depth (z) of the vehicle was sensed using a pressure transducer. Measurements of pitch and roll were provided by a dual-axis inclinometer. Heading was measured using a flux-gate compass. Solid-state gyros were used to provide pitch, roll, and yaw angular rates. Each of these sensors is commercially available.

3 Approach

Dynamically Coordinated Control

The central idea of the dynamically-coordinated-control approach is to take advantage of physical understanding of system dynamics explicitly in the control of the arm/vehicle system. In the context of the control problem addressed here, this physical understanding is embodied in an accurate model of the manipulator hydrodynamic forces. Under the coordinated-control approach, hydrodynamic and inertial forces generated from the motion of the arm are modeled in real time as the motion progresses. Based on the predicted interaction forces, thrust commands are sent to the thrusters to counteract the forces generated by the arm motion. In this way, the control of the arm and the vehicle are "coordinated."

Figure 3 shows a simplified schematic diagram of the coordinated-control strategy. The main control components are the hydrodynamic model, the arm controller, the vehicle controller, the arm trajectory generator, and the vehicle trajectory generator. The control approach presented here was developed with the availability of an accurate hydrodynamic model in mind. The primary advantage of using a model to predict the hydrodynamic forces acting was increased reliability and simplicity — no additional sensors were required.

Hydrodynamic Model

The experimental validation of the coordinated-control approach of this paper was enabled, in part, by the development of a very accurate hydrodynamic model for the in-line forces acting on a circular cylinder *swinging* about its end. The theoretical foundation of this model is a two-dimensional analysis of the flow of an incompressible, inviscid fluid over a cylinder accelerating from a stop. The wake and feeding layers were modeled using discrete vortices.

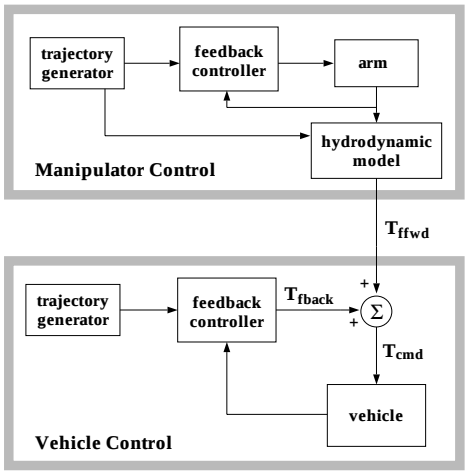

Figure 3: Coordinated-Control Block Diagram

The 2-D analysis resulted in the following equation for the acting hydrodynamic *in-line* force.

$$\begin{aligned} F_X &= -C_m(s/D) \cdot \rho \frac{\pi D^2}{4} \frac{dU}{dt} \\ &\quad -C_d(s/D) \cdot \frac{1}{2} \rho D U^2 \end{aligned} \tag{1}$$

where D is the diameter, s is the displacement, and U is the velocity of the cylinder, and ρ is the fluid density. The key outcome of this analysis was that for a cylinder undergoing constant acceleration motions, it was found that the time-varying hydrodynamic drag and added-mass coefficients, C_d and C_m, were functions of how far the cylinder had traveled *only*.

Using a standard strip-theory approach, the 2-D analysis was extended to three dimensions. This approach is diagrammed in Figure 4. The forces acting on a thin segment of the arm were calculated using a form of equation 1.

$$\begin{aligned} dF_i &= -C_{m_i}(s_i/D) \cdot \rho \frac{\pi D^2}{4} l_i dl_i \ddot{\theta} \\ &\quad -C_{d_i}(s_i/D) \cdot \frac{1}{2} \rho D l_i^2 dl_i |\dot{\theta}| \dot{\theta} \end{aligned} \tag{2}$$

The hydrodynamic in-line torque and force acting at the hub were found using the following simple relations:

$$dT_i = l_i dF_i \tag{3}$$

$$T_{hyd} = \sum_{i=1}^{n} dT_i \tag{4}$$

$$F_{hyd} = \sum_{i=1}^{n} dF_i \tag{5}$$

where n was the number of segments used in the model.

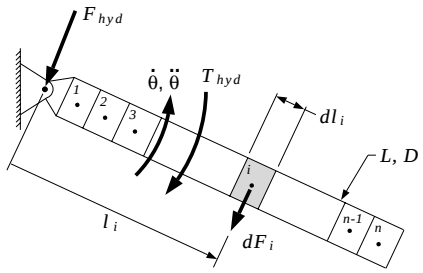

Figure 4: Strip-Theory Implementation

Extensive measurements of forces and torques acting on the arm were used to identify the time-varying behavior of C_d and C_m. Flow visualization studies were also conducted to gain insight into the behavior of the flow and its effects on the forces acting. The hydrodynamic coefficients for a cylinder *swinging* from one position to another were found to vary significantly from those for a cylinder undergoing steady translational motions. Full details of the hydrodynamic model, including the time-varying behavior of the drag and added-mass coefficients can be found in [8].

Figure 5 demonstrates the accuracy of the hydrodynamic model based on Equations 2, 3, and 4. It can be seen that for a wide range of motions, that the model accurately predicts the hydrodynamic torque acting.

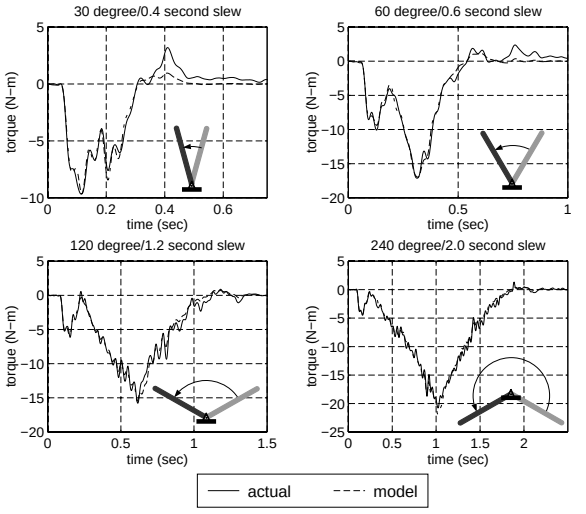

Figure 5: Hydrodynamic Modeling Results

Vehicle Feedback Control System

For the fairly low speeds characteristic of station-keeping operation, the motion of the independent degrees of freedom of the vehicle are very lightly damped. This is due to the signed-quadratic relationship between velocity and fluid drag. At very low speeds, the drag is almost non-existent. At high speeds the drag forces are extremely large. For the low speeds involved in station keeping, the x, y, and z translational motions and the yaw motion can be modeled approximately as $1/s^2$ plants, while the pitch and roll motions can be modeled as lightly damped second order systems.

To provide control over the individual vehicle degrees of freedom, classical proportional-integral-derivative (PID) feedback controllers were used. The integral portion of the control was implemented so that it was only active when the desired vehicle velocity was zero. In this way, good steady state error performance was achieved while preserving good transient response. Figure 6 shows a schematic representation of the vehicle feedback control implemented on the OTTER vehicle. The control loop was implemented digitally with a 100 Hz update rate. However, x and y position information from SHARPS was available at only 3 Hz. Yaw information from the flux-gate compass was produced at 10 Hz.

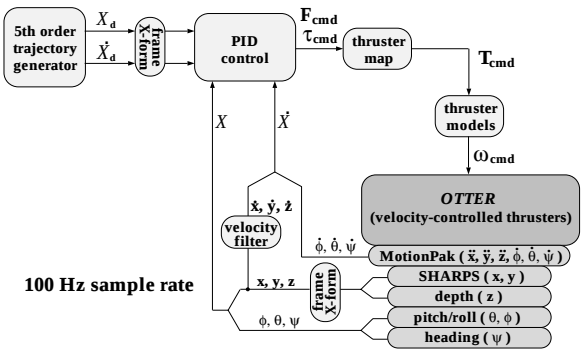

Figure 6: Vehicle Control Block Diagram

For station-keeping operations, the vehicle trajectory generator produced constant desired-position commands. Based on errors, the vehicle controller produced a vector of three forces $[F^x_{cmd} \;\; F^y_{cmd} \;\; F^z_{cmd}]^T$ and three torques $[\tau^x_{cmd} \;\; \tau^y_{cmd} \;\; \tau^z_{cmd}]^T$ to be applied to the vehicle about its center of gravity in the vehicle frame. From F_{cmd} and τ_{cmd}, a vector of eight thrust commands (T_{cmd}) for the vehicle were calculated using a thruster mapping matrix.

Good agreement between the commanded thrust and the actual thrust produced by the thrusters was achieved by controlling the thruster motors in velocity mode and taking advantage of the steady-state relationship between thrust pro-

duced and the angular velocity of the output shaft:

$$\omega_{cmd} = k_T sgn(T_{cmd})\sqrt{|T_{cmd}|} \qquad (6)$$

where k_T is a calibration constant determined for each of the thrusters.

In the absence of arm motion, good positioning performance was achieved using PID control on the individual degrees of freedom of the vehicle.

Arm Feedback Control System

Figure 7 shows a schematic block diagram of the arm controller implemented for the experiments described in this paper. This implementation takes advantage of the 1 kHz, high-gain velocity feedback controller internal to the motor electronics. By controlling the arm motor in "velocity control" mode, the arm actuator behaved as a velocity source.

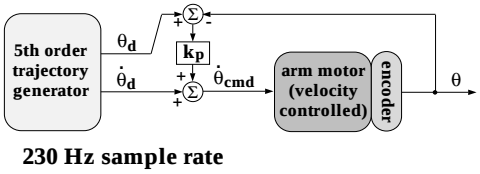

Figure 7: Arm Control Block Diagram

A fifth-order trajectory generator was used to provide smooth desired commands to the controller. Desired velocity commands direct from the trajectory generator were sent to the motor as feedforward signals. A proportional position feedback loop was closed around the internal velocity feedback loop to provide control of the arm joint angle. Because of the well-damped dynamic characteristics of the arm, high position feedback gains were achievable and very good position control was attained.

Coordinated-Control Implementation

Feedback controllers were applied to the arm and vehicle as described above. In addition, the hydrodynamic model and feedforward connection were added to complete the coordinated-control implementation as shown in Figure 3. The essential information for implementation of the hydrodynamic model were the position, velocity, and acceleration of the link relative to the water. In providing this information, three simplifying assumptions were made: 1) vehicle motions were small and did not contribute significantly to the motion of the manipulator relative to the water, 2) desired joint acceleration was a good approximation of the actual joint acceleration, and 3) the water through which the arm was moving was still.

The output of the hydrodynamic model was a vector of three forces $[F^x_{hyd}\ F^y_{hyd}\ F^z_{hyd}]^T$ and three torques $[\tau^x_{hyd}\ \tau^y_{hyd}\ \tau^z_{hyd}]^T$ acting about the base of the arm joint. These were the forces and torques required to counteract the forces generated by the motion of the arm. As with the feedback control, a thruster configuration map was used to determine the required feedforward commands to the thrusters (T_{ffwd}) to counteract the hydrodynamic coupling forces.

Feedforward thrust commands were sent to the vehicle controller 60 times per second over an Ethernet connection between the arm and vehicle card cages. These feedforward commands were summed directly with the feedback commands, T_{fback}, to produce the the total thrust command to be sent to the thrusters, T_{cmd}.

Combining feedback control with feedforward control resulted in a vehicle controller that possessed the positive attributes of both types of control. Feedback control provides regulation capability, robustness to disturbances, and robustness to plant model uncertainties. Feedforward control provides rapid dynamic response by taking advantage of information from models of the known system dynamics. Rather than waiting for an error to build up, feedforward control predicts what the control command should be to regulate the errors in the system *before* the errors occur. For the problem considered here, a combination of feedforward control and feedback control provided the best solution.

Experimental Test Strategy

To determine the value of the proposed coordinated-control strategy, four different vehicle controllers were implemented and tested. In each of the four evaluated vehicle controllers, the arm control used was identical (see Figure 7).

- *No Vehicle Control.* In this case, both the feedforward path from the arm hydrodynamic model and the vehicle feedback control loop were open.

- *Feedback Control Only.* In this control configuration, the vehicle feedback control loop was closed while the feedforward path from the arm model to the vehicle remained open.

- *Feedforward Control Only.* In this implementation, the vehicle feedback control loop remained open while the feedforward path from

the hydrodynamic model to the vehicle was closed.

- *Combined Feedforward & Feedback Control.* In this case, both the vehicle feedback control loop and the feedforward path from the arm model were closed.

The Feedback Control Only test case, along with the No Vehicle Control case, provided performance baselines against which the Combined Feedforward & Feedback Control approach was compared.

4 Experimental Results

In this section, several different types of data are presented including vehicle station-keeping data, arm end-point positioning data, and arm end-point rise-time data. Using these results, comparisons are drawn between the different controller types. The results demonstrate the benefits of both feedback control and feedforward control and their complementary attributes that result in the best control behavior when feedback and feedforward control are combined.

Vehicle Station Keeping

To compare the station-keeping performance of the different vehicle controllers, selected vehicle roll and yaw angle data are presented. In this particular application, roll and yaw were the degrees of freedom most affected by the hydrodynamic coupling between the arm and the vehicle. Figure 8 shows a typical time history of the joint angle for the multiple-swing arm motions executed for the vehicle station-keeping tests.

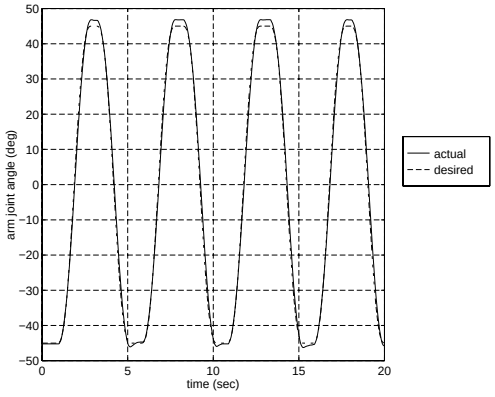

Figure 8: Arm-Joint-Angle Time History

Vehicle Roll Error Figure 9 shows time histories of vehicle roll error data for each of the four controller types considered. With no control effort, roll errors were very large (between ±18 degrees) as the open-loop roll mode of the vehicle was excited. The addition of feedback control improved the roll error regulating performance, but the errors were still significant (between ±9 degrees). Feedforward control alone effectively countered much of the roll moment generated from the arm motion. In this case, feedforward control allowed the vehicle to respond to arm interaction forces that were beyond the bandwidth where the feedback control was most effective, but within the bandwidth of the thrusters. Further improvement was realized when feedforward and feedback control were combined. Peak roll errors were limited to less than 1.5 degrees in this case.

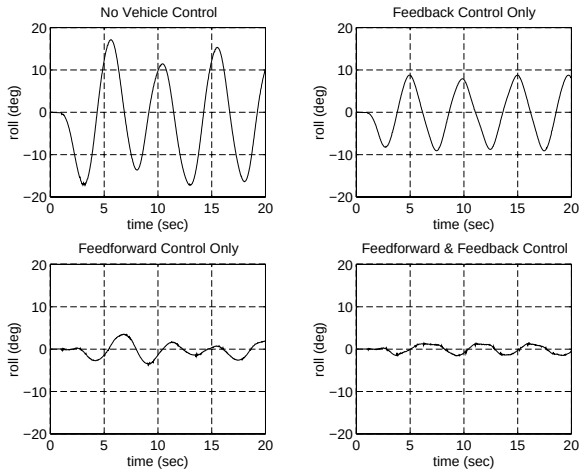

Figure 9: Vehicle Roll Error Versus Time

Vehicle Yaw Error Time histories of vehicle yaw error for the different controllers are shown in Figure 10. When no feedback or feedforward control was applied, the vehicle heading angle drifted significantly from its nominal position. Unlike the roll and pitch attitude degrees of freedom, the yaw degree of freedom has no passive restoring force inherent to its open-loop dynamics. Because of this, the yaw degree of freedom was fully dependent on feedback control to prevent drifting due to disturbances or uncertainty in the plant model. When feedback control alone was applied, the tendency to drift was reduced, but the closed-loop dynamics of the yaw controller became apparent. As the controller attempted to reject the yaw disturbance, it caused the vehicle to oscillate significantly in response (up to 9 degrees error). When

only feedforward control was applied, the yaw disturbance due to arm motion effectively was cancelled resulting in much smaller yaw errors. With feedback and feedforward control combined, the yaw errors were again small. Yaw errors were roughly three times smaller for the Feedforward Only and Feedforward & Feedback cases than for the Feedback Only case.

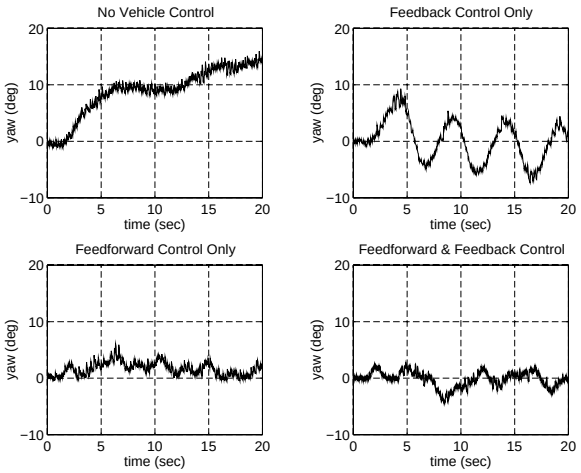

Figure 10: Vehicle Yaw Error Versus Time

End-point Positioning

While not sensed and controlled directly in these experiments, arm end-point position error is a useful indicator of the quality of the performance of the arm/vehicle controller. End-point position data were generated by post-processing vehicle position and attitude and arm position measurements based on the kinematic configuration of the system. Data sampling on the vehicle controller and arm controller was synchronously triggered to allow correlation of arm and vehicle data in time.

For the multiple-swing motions of the arm, Figure 11 shows time histories of the arm end-point error for the four controllers tested. The mean end-point errors were calculated to be 0.28 m for the No Vehicle Control case, 0.11 m for the Feedback Control Only case, 0.091 m for the Feedforward Control Only case, and 0.046 m for the Feedforward & Feedback Control case. It can be seen that with combined feedforward and feedback control, that the end-point errors were reduced by a factor of six when compared with the No Vehicle Control case and a factor of 2.5 when compared to the Feedback Control Only case.

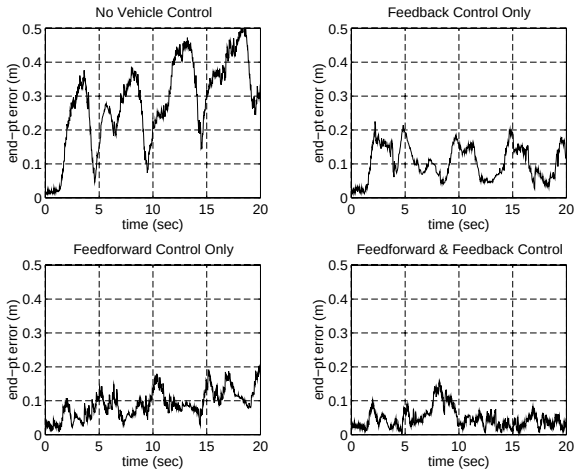

Figure 11: End-Point Error — Multiple Swings

End-point Settling-Time

Figure 12 shows plots of the distance of the arm end point from the desired target for the four different controllers. This data was obtained by slewing the arm through 90 degrees in two seconds. For the slews considered, the distance traveled by the end point was about 1.5 m. Here settling time is defined as the time required to move and stay within five percent (of the total distance traveled) of the target — in this case ± 0.075 m.

These settling-time plots demonstrate the importance of the feedback component of the vehicle control. Without feedback, the arm end point either fails to come within five percent of the target (as in the No Vehicle Control case) or it fails to remain within the five-percent error bound around the target point (as in the Feedforward Control Only case).

In the Feedback Control Only case, the time required to settle to within five percent of the target was about 6.5 seconds. As the arm moved, significant errors in roll, yaw, x, and y resulted. Coming and staying within the error bound required these errors to be reduced which took a substantial amount of time.

In the Feedforward & Feedback Control case, the observed settling time was about two seconds. This represents an improvement of over three times compared to the settling time of the Feedback Control case. Because the vehicle stayed on station, the settling time corresponded directly to the duration of the slew.

It is important to note that the performance improvements demonstrated here were achieved with only a moderate increase in total thrust used [8]. This was made possible by taking advantage of

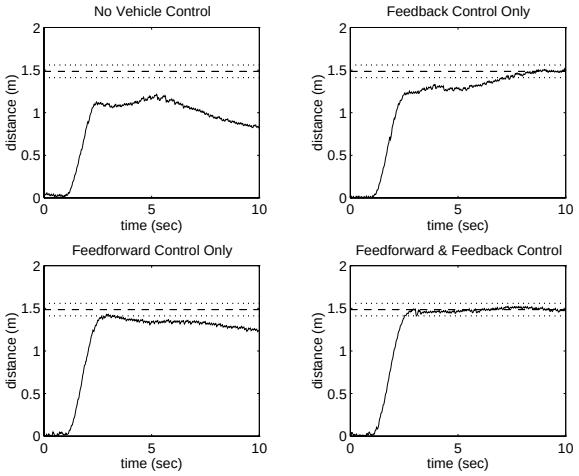

Figure 12: End-Point Settling Time

knowledge of the system dynamics and coordinating the control in a sensible way.

5 Conclusions

In this paper, an intuitively straightforward approach developed for the coordinated control of an underwater arm/vehicle system has been described in detail. Experiments demonstrated that the hydrodynamic coupling forces between an arm and a vehicle can be very significant, resulting in large disturbances to the station-keeping control of the vehicle. Experimental results showed that substantial performance improvements can be realized in the control of an underwater arm/vehicle system by incorporating model-based feedforward information about the hydrodynamic coupling into the control of the system. Tracking errors at the manipulator end point were typically reduced by over a factor of six using the coordinated control approach when compared to the vehicle with no control applied and by a factor of 2.5 when compared to the standard approach of independent arm and vehicle feedback controllers. Using the approach presented here, settling times at the manipulator end point were also reduced by over three times when compared to the values obtained using feedback control alone. These dramatic performance improvements were achieved with only a moderate increase in control effort.

6 Acknowledgments

This research was supported by the Monterey Bay Aquarium Research Institute, ONR Contract N0014-92-J-1943, and NASA Contract NCC 2-333.

References

[1] H. H. Wang, R. L. Marks, S. M. Rock, and M. J. Lee. Task-Based Control Architecture for an Untethered, Unmanned Submersible. In *Proceedings of the 8th Annual Symposium of Unmanned Untethered Submersible Technology*, pages 137–147. Marine Systems Engineering Laboratory, Northeastern University, September 1993.

[2] Dana R. Yoerger and Jean-Jaques E. Slotine. Robust trajectory control of underwater vehicles. *IEEE Journal of Oceanic Engineering*, OE-10(4):462–470, 1985.

[3] Anthony J. Healey and David Lienard. Multivariable sliding-mode control for autonomous diving and steering of unmanned underwater vehicles. *IEEE Journal of Oceanic Engineering*, 18(3):327–339, 1993.

[4] Roberto Cristi, Fotis A. Papoulias, and Anthony J. Healey. Adaptive sliding mode control of autonomous underwater vehicles in the dive plane. *IEEE Journal of Oceanic Engineering*, 15(3):152–160, 1990.

[5] Junku Yuh. A neural net controller for underwater robotic vehicles. *IEEE Journal of Oceanic Engineering*, 15(3):161–166, 1990.

[6] H. Mahesh, J. Yuh, and R. Lakshmi. A coordinated control of an underwater vehicle and robotic manipulator. *The Journal of Robotic Systems*, 8(3):339–370, 1991.

[7] H. H. Wang, R. L. Marks, T. W. McLain, S. D. Fleischer, D. W. Miles, G. A. Sapilewski, S. M. Rock, M. J. Lee, and R. C. Burton. OTTER: a testbed submersible for robotics research. In *Proceedings of the ANS 6th Topical Meeting on Robotics and Remote Systems*. American Nuclear Society, February 1995.

[8] Timothy W. McLain. *Modeling of Underwater Manipulator Hydrodynamics with Application to the Coordinated Control of an Arm/Vehicle System*. PhD thesis, Stanford University, July 1995. Under preparation.